Available online at www.sciencedirect.com
SCIENCE DIRECT
Journal of Solid State Chemistry 179 (2006) 1995–2003
JOURNAL OF SOLID STATE CHEMISTRY
www.elsevier.com/locate/jssc

Er^{3+}-doped PbF_2: Comparison between nanocrystals in glass-ceramics and bulk single crystals

G. Dantelle[a], M. Mortier[a,*], G. Patriarche[b], D. Vivien[a]

[a]Laboratoire de Chimie Appliquée de l'Etat Solide, CNRS-UMR 7574, ENSCP-11, rue Curie-F-75005 Paris, France
[b]Laboratoire de Photonique et de Nanostructures, CNRS-UPR20, route de Nozay-F-91460 Marcoussis, France

Received 31 January 2006; received in revised form 24 March 2006; accepted 27 March 2006
Available online 1 April 2006

Abstract

An appropriate annealing of a GeO_2–PbO–PbF_2:ErF_3 glass leads to the formation of a glass-ceramic, composed of $Pb_{1-x}Er_xF_{2+x}$ nanosized crystallites dispersed throughout an amorphous oxide matrix. These nanocrystallites are compared to Er^{3+}-doped PbF_2 bulk single crystals. The influence of the annealing temperature on the glass-ceramics characteristics is thoroughly investigated. For several glass-ceramics resulting from different heat treatments, the quantity of crystallized PbF_2, as well as the segregation of Er^{3+} ions into the crystallites, has been studied through two methods: first, the study of the crystallographic characteristics and second, the evolution of the optical properties. It was evidenced that, for a heat treatment over 365 °C, the whole PbF_2:Er has completely crystallized and that the segregation of Er^{3+} ions into the crystallites was total. Strong interactions between Er^{3+} ions occur in the $Pb_{1-x}Er_xF_{2+x}$ single and nanocrystals, promoting cross-relaxation processes, under 488-nm excitation, and favouring the 660- (red) and 810-nm emissions at the expense of the 550-nm (green) one.

Keywords: Oxyfluoride glass-ceramics; Nanoscale; Rare-earth; Annealing; Nucleation/growth; Fluorescence; Lifetime

1. Introduction

Transparent rare-earth-doped glass-ceramics have been studied for their optical properties, with the aim of developing a new class of optical amplifiers [1]. Indeed, laser emission has already been observed in Nd^{3+}-doped alumino-silicate glass-ceramics [2,3]. Glass-ceramics are composite materials, lying between glasses and crystals, and combining the good optical and mechanical properties of crystals with the easy shaping ability of glasses. They are synthesized from glasses that are annealed for appropriate time and temperature to enable the formation of crystallites inside the glass. The annealing step, depending on the glasses composition, needs to be well controlled to obtain a high-quality material, i.e. a glass-ceramic:

(a) with nanosized crystallites to keep a good transparency of the material [4],
(b) with the complete crystallization of the wanted phase,
(c) with a total segregation of the active ions (RE ions) into the crystalline phase to optimize the optical properties (to narrow the inhomogeneous linewidth for instance).

We are studying the $50GeO_2$–$40PbO$–$10PbF_2$ system doped with ErF_3, as it appears to be a potential candidate for 1.54-μm optical fibre amplifier. In such system, the crystalline phase is lead fluoride and the glassy phase is composed of mixed oxides. It has been demonstrated [5–8] that ErF_3 behaved as a nucleating agent for the cubic β-PbF_2 phase and that, consequently, Er^{3+} ions were incorporated into the crystallites, forming a $Pb_{1-x}Er_xF_{2+x}$ solid solution. These oxyfluoride glass-ceramics are particularly interesting for their optical properties as the fluoride environment of the rare-earth, with its low phonon energy, contributes to reduce the non-radiative de-excitations, leading to an improved quantum efficiency of the radiative emission with respect to an oxide environment. Nonetheless, the real content of Er^{3+} ions incorporated

*Corresponding author. Fax: +33 1 46 34 74 89.
E-mail address: michel-mortier@enscp.fr (M. Mortier).

0022-4596/$ - see front matter © 2006 Elsevier Inc. All rights reserved.
doi:10.1016/j.jssc.2006.03.038

into the crystallites, as well as the actual quantity of crystallized PbF_2, has never been precisely studied in the literature.

In this paper, we report a detailed investigation of the evolution of the fluoride phase crystallization in glass-ceramics and of the segregation of Er^{3+} ions into the crystallites, through two complementary methods: first, the study of the crystallographic characteristics of the glass-ceramics and second, the study of the optical properties of those glass-ceramics. For sake of comparison, the crystallographic and optical characteristics of β-PbF_2 bulk single crystals doped with various percentage of ErF_3 were also investigated and compared to those of the glass-ceramics.

2. Experimental section

A glass was synthesized with the molar composition $50GeO_2$–$40PbO$–$10PbF_2$:$2ErF_3$. In the following, the sample will be labelled GPF:2Er. The first step of the synthesis was to mix high purity powders (GeO_2: 99.999%, PbO: 99%, PbF_2: 99.997%, ErF_3: 99.99%). This mixture was then heated for 20 min at 1050 °C in air. Finally, it was poured on a copper plate previously heated at 150 °C and covered by another copper plate to obtain the glass. The Differential Thermal Analysis (DTA) of the glass was carried out on a symmetric analyzer TAG24 (SETARAM, France) under argon flux, using 60 mg of powder sifted between 45 and 71 μm. The heating rate was 10 °C/min.

β-PbF_2 bulk single crystals doped with ErF_3 were synthesized by a modified Bridgman technique, under argon atmosphere. PbF_2 and ErF_3 powders were put in a vitreous carbon crucible, in the strong thermal gradient (20 °C/cm) of a vertical furnace. The temperature of the furnace was set at 1000 °C for 20 min and was then decreased very slowly (10 °C/h). Due to the thermal gradient, the top of the mixture was cooler than the down. Without any physical displacement, the low cooling rate of the furnace allowed the displacement of the thermal gradient and then of the crystallization front from the top to the down of the crucible. Finally, 3-cm-long single crystals of solid solutions $Pb_{1-x}Er_xF_{2+x}$, with $x = 0.002$, 0.02, 0.09 and 0.20, were obtained.

X-ray diffraction (XRD) measurements were performed on a Siemens D5000 diffractometer, using a Co anode ($\lambda_{Co} = 1.789$ Å).

Transmission electron microscopy (TEM) was carried out on a 200-kV Philips CM20 microscope. The samples were ground in ethanol and placed onto a carbon-coated copper grid for introduction into the microscope.

The fluorescence decay curves around 1.5 μm were performed under pulsed excitation using an optical parametric oscillator (OPO), pumped by the third harmonic of a Q-switched Nd^{3+}-YAG laser (355 nm). A filter, transparent to the radiations over 1130 nm, was placed at the entrance of an InGaAs cell connected to a digital oscilloscope. As the InGaAs detector does not operate above 1.8 μm, only the 1.5-μm fluorescence, resulting from the $^4I_{13/2}$ energy level radiative de-excitation, was collected. Because of the broad wavelength detection range, no site selectivity was induced when measuring the $^4I_{13/2}$ level lifetime. The measurements were done on thin powder films, in order to avoid reabsorption effects.

The visible and near infra-red fluorescence spectra were recorded under an Ar ion laser excitation at 488 nm and analyzed through a 250-mm monochromator fitted with a photomultiplier.

3. Results and discussion

3.1. Crystallization rate

3.1.1. DTA study

The DTA curve of the GPF:2Er glass is presented in Fig. 1. The vitreous transition T_g corresponds to the inflexion point situated at 345 °C. The first exothermic peak, centred at 405 °C, corresponds to the crystallization of the β-PbF_2 phase, labelled $T_c(\beta\text{-}PbF_2)$. The two other exothermic peaks, situated at 503 and 537 °C, correspond to the crystallization of two oxide phases, respectively, $PbGeO_3$ and $PbGe_4O_9$ [9]. Finally, the broad endothermic peaks, in the 600–700 °C range, correspond to the fusion of PbF_2 and of the mixed oxides.

Eight glass samples were cut and each one was annealed for 10 h at a different temperature: 350, 355, 360, 365, 370, 380, 385 and 395 °C. The glass-ceramics resulting from these different heat treatments were analyzed by DTA. The DTA curves, in the temperature range 300–490 °C, of the glass and of some glass-ceramics are shown on Fig. 2a. One can notice that the area of the crystallization peak of PbF_2, hachured in Fig. 2a, decreases as the annealing temperature increases. It indicates that the heat treatment induces the crystallization of the PbF_2 phase. For annealing temperatures over 360 °C, the PbF_2 crystallization peak

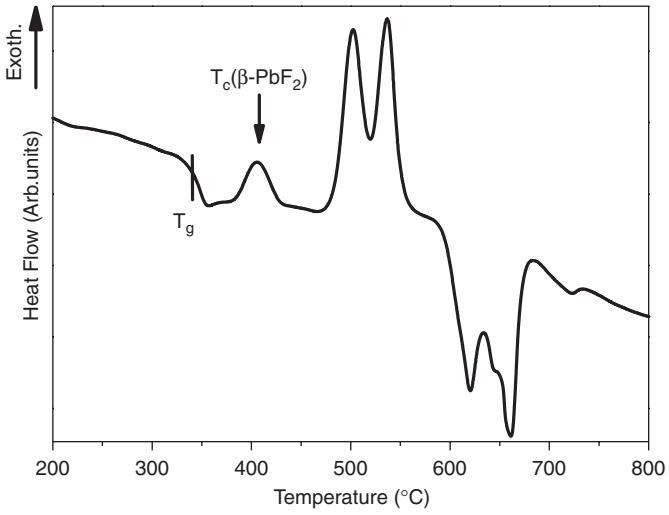

Fig. 1. DTA curve of the glass sample GPF: 2Er. T_g and $T_c(\beta$–$PbF_2)$ indicate, respectively, the vitreous transition temperature and the crystallization temperature of β-PbF_2.

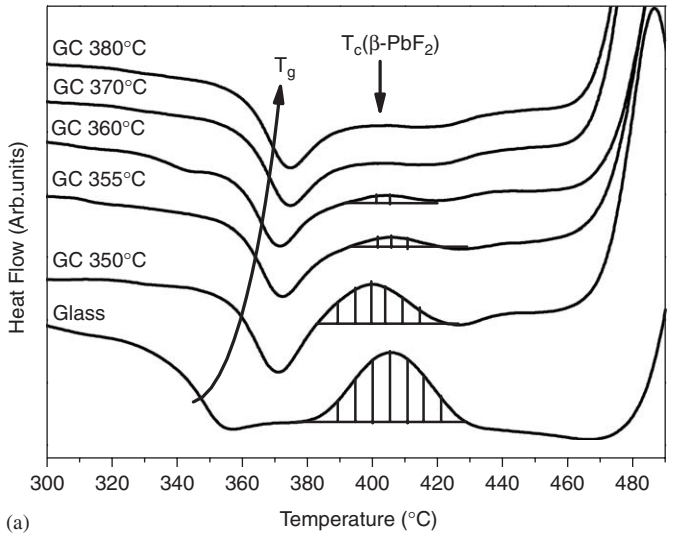

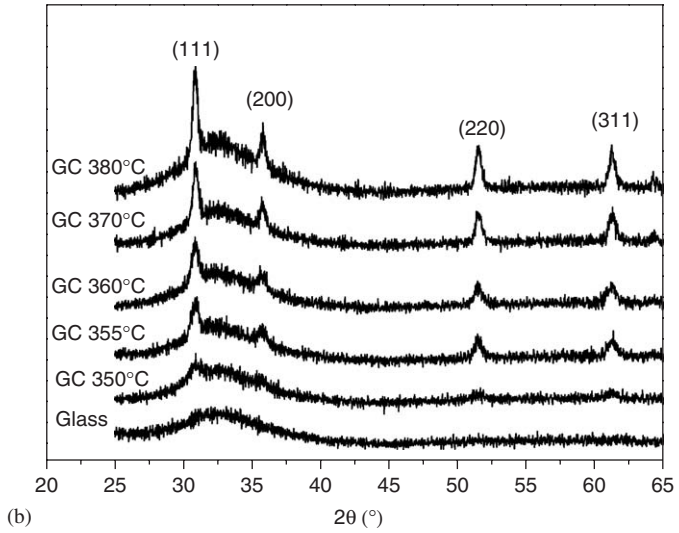

Fig. 2. DTA curves (a) and XRD diagrams (b) of the glass and of the glass-ceramics (GC) resulting from the different heat treatments. The hachured area of the DTA curves represents the quantity of PbF_2 remaining in the glass A_{glass} or in the glass-ceramics, A_{GC}.

had completely disappeared, indicating that all the PbF_2 had been crystallized in the glass-ceramics.

The evolution of the crystallization peak of PbF_2, as a function of temperature, enables one to follow the crystallization of the fluoride phase. Indeed, using these DTA curves, a crystallization rate of PbF_2 in the glass-ceramics, labelled R_{DTA}, is introduced. It is calculated by the expression:

$$R_{DTA} = \frac{A_{glass} - A_{GC}}{A_{glass}} \times 100,$$

where A_{glass} is the area of PbF_2 crystallization peak in the glass and A_{GC} is the area of the crystallization peak of PbF_2 in the glass-ceramics. The values of R_{DTA} are gathered in Table 1 for all the glass-ceramics. R_{DTA} increases from 0% in the glass to 100% (for complete crystallization of the PbF_2 phase) when the annealing temperature is over 360 °C.

Table 1
Crystallographic parameters of the different glass-ceramics according their annealing temperature

Annealing temperature (°C)	R_{DTA} (%)	R_{XRD} (%)	a (Å)	L (nm)
Glass	0	0	—	—
350	41±4	9±3	5.828±0.005	11.0±1
355	76±4	21±2	5.827±0.005	15.8±1
360	81±4	22±2	5.827±0.005	16.2±1
365	100	26±2	5.830±0.005	19.8±1
370	100	26±2	5.823±0.005	20.0±1
380	100	25±2	5.826±0.005	22.0±1.5
385	100	25±2	5.822±0.005	23.5±1.5
395	100	26±2	5.824±0.005	26.3±1.5

Moreover, in Fig. 2a, one can notice that the increase of the annealing temperature induces a slight shift of the vitreous transition T_g of the glass-ceramics towards higher temperatures, revealing that the glassy phase of the glass-ceramics becomes more and more stable. In fact, the amount of PbF_2 that remains in the glass decreases when the annealing temperature increases. Consequently, there are less non-bridging fluorine ions in the glassy phase, inducing an increase of the glassy phase stability [10].

3.1.2. XRD study

XRD diagrams of the glass-ceramics resulting from the different heat treatments were carried out and some of them are represented in Fig. 2b. One can observe the diffraction peaks of the cubic β-PbF_2 phase, superimposed on the diffuse scattering of the amorphous phase. The intensity of the diffraction peaks increases with the increase of the annealing temperature, while the diffusion band area decreases indicating the progressive crystallization of the PbF_2 phase.

From these diagrams, a crystallization ratio R_{XRD} expressed as

$$R_{XRD} = \frac{\text{Area of the diffraction peaks}}{\text{Total area of the XRD diagram}}$$

was calculated. This ratio enables to evaluate roughly the PbF_2 crystallization rate in the glass-ceramics. In the above expression, the considered diffraction peaks are those situated between $2\theta = 25°$ and 65° and the total area is calculated in the same 2θ range. This ratio allows a qualitative and convenient approach of the PbF_2 crystallization rate, but, in no case, a quantitative evaluation. The R_{XRD} values, gathered in Table 1, increases when the annealing temperature increases up to 365 °C. For annealing temperatures over 365 °C, R_{XRD} remains constant around 26%, meaning that the fraction of crystallized PbF_2 does not vary any more.

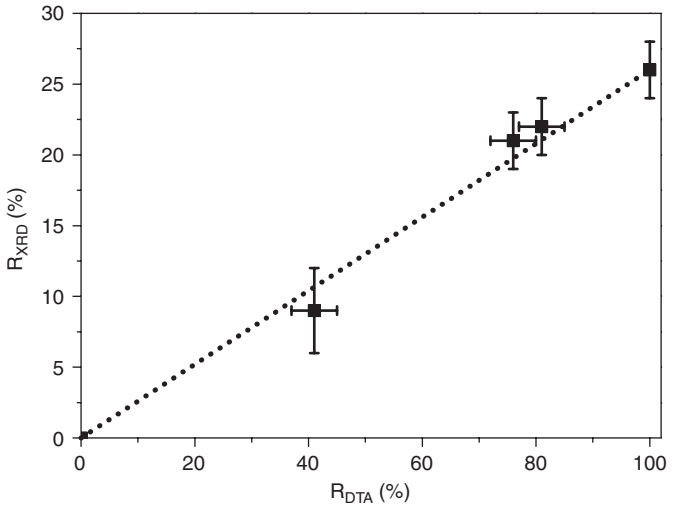

Fig. 3. Correlation between the crystallization rate R_{XRD} calculated by X-ray diffraction and the crystallization rate R_{DTA} calculated by differential thermal analysis.

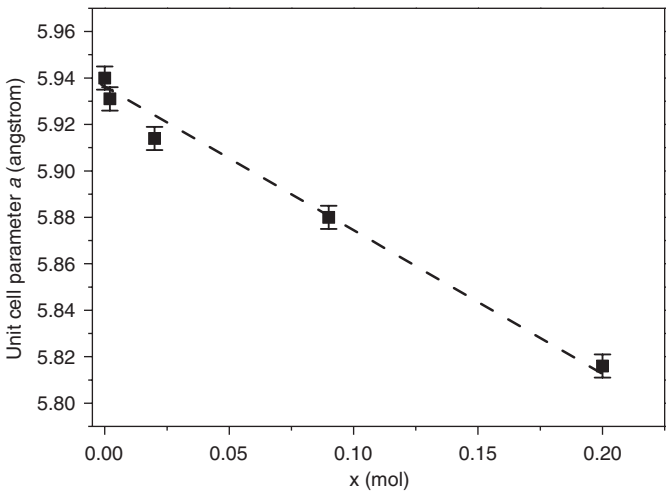

Fig. 4. Evolution of the $Pb_{1-x}Er_xF_{2+x}$ bulk single-crystal unit cell parameter according to the Er^{3+} doping rate, x.

3.1.3. Correlation between DTA and XRD measurements

The evolution of the crystallization rate of the fluoride phase, followed by the calculation of R_{XRD} and R_{DTA} (Table 1), is similar. When the annealing temperature increases, the PbF_2 crystallization rates increases, up to a constant value of either 26% for R_{XRD} or 100% for R_{DTA}. A correlation between these two measurements is presented in Fig. 3. Such a correlation enables to calibrate the values obtained by R_{XRD} and to deduce that an $R_{XRD} = 26\%$ corresponds to a complete crystallization of the PbF_2 phase. Hence, for annealing temperatures lower than 365 °C, the crystallization of PbF_2 is not complete; but for higher annealing temperatures, all the PbF_2 of the starting glass has crystallized throughout the glass-ceramic.

These two methods used for the calculation of the PbF_2 crystallization rate are complementary. Indeed, for high crystallization rates, the method using XRD diagrams for the calculation of the crystallization rate is well adapted as the PbF_2 diffraction peaks are well defined, while the A_{GC} values are small, whereas at low crystallization rates, it is much easier to use the DTA curves.

3.2. Segregation of Er^{3+} ions into the β-PbF_2 phase

The β-PbF_2 unit cell parameter a in the glass-ceramics and bulk single crystals was calculated from the position of the diffraction peaks of the XRD diagrams. It is given in Table 1 for the glass-ceramics and shown in Fig. 4, as a function of the doping rate, for the single crystals.

3.2.1. Influence of the Er^{3+} doping rate on the a parameter value of the PBF_2 bulk single crystals

The unit cell parameter of the $Pb_{1-x}Er_xF_{2+x}$ bulk single crystals linearly decreases from 5.940 Å for $x = 0$ to 5.816 Å for $x = 0.20$ as shown in Fig. 4. Similar evolution was already observed [11] in the case of Yb^{3+}, Ho^{3+}, Nd^{3+} and Gd^{3+} doping in β-PbF_2, up to the rare-earth solubility limit. The a values are always much smaller than the unit cell parameter of pure β-PbF_2 ($a = 5.94$ Å) [12], proving the substitution of Pb^{2+} by Er^{3+} inside the β-PbF_2 unit cell. Despite the presence of an interstitial F^- ion insuring the charge balance associated with the Pb^{2+}/Er^{3+} substitution, the reduction of the ionic radius from Pb^{2+} (1.45 Å in eight-fold coordination) to Er^{3+} (1.14 Å in eight-fold coordination) dominates and explains the decrease of the unit cell parameter [13]. Smaller the ionic radius of the Ln^{3+} ion, smaller the $Pb_{1-x}Ln_xF_{2+x}$ unit cell parameter [11].

The experimental density of the $Pb_{0.8}Er_{0.2}F_{2.2}$ bulk single crystal, measured through the Archimedes' principle, is equal to $d_{exp} = 8.09 \pm 0.02$. Assuming the above formula and the a parameter value of 5.816 ± 0.005 Å, one calculates $d_{th} = 8.14 \pm 0.02$. The similarity of the measured and calculated densities confirms that the bulk single-crystal formula is indeed the expected one.

3.2.2. Independence of the PbF_2 a parameter as a function of the annealing temperature of the glass-ceramic

Whatever the annealing temperature, the unit cell parameter a of the $Pb_{1-x}Er_xF_{2+x}$ nanocrystallites in the glass-ceramics (Table 1) is almost constant, with an average value of $a = 5.826 \pm 0.005$ Å. It indicates that the crystallites composition, and more particularly their Er^{3+} content, is the same in each glass-ceramic whatever the crystallization rate may be. β-PbF_2 phase crystallizes in incorporating progressively the Er^{3+} ions at a constant rate. This is in agreement with the nucleation growth theories evidencing an invariant chemical composition of the separated phases during the whole process [5], which is opposite to the spinodal decomposition.

3.2.3. Comparison of the unit cell parameter of the bulk single crystals and the glass-ceramics

The idea was to compare the unit cell parameter of the nanocrystallites of the glass-ceramics to the unit cell parameter of the $Pb_{1-x}Er_xF_{2+x}$ bulk single crystals in order to deduce the crystallites composition. But, this method is possible only if, in the glass-ceramics, the amorphous matrix does not affect the crystallites unit cell parameter because of strains and pressure [14]. Indeed, such a phenomenon would prevent the comparison between the nanocrystallites of the glass-ceramics and the bulk crystals. To ensure the validity of the study, the amorphous matrix of one of the studied glass-ceramics was selectively dissolved in hydrofluoric acid [15]. The nanocrystallites were then filtered and their unit cell parameter was then determined. It was found to be identical with before the dissolution, as well as the crystallites size. Hence, no modification of the unit cell parameter and of the crystallites size is induced by the oxide matrix.

The unit cell parameter a of the nanocrystallites of the glass-ceramics ($a = 5.826 \pm 0.005$ Å) corresponds to a $Pb_{0.82}Er_{0.18}F_{2.18}$ composition inside the crystallites, according to the bulk single-crystal unit cell parameter evolution (Fig. 4). It means that, in the glass-ceramics, the crystallites contain Pb^{2+} and Er^{3+} ions in the ratio $Er/Pb = 0.21$, i.e. $ErF_3/PbF_2 = 0.21$ at each time of the nucleation/growth process. In the starting glass, the ratio ErF_3/PbF_2 was 0.2, which is identical (accounting for the measurements uncertainties) with the one found in the crystallites. Hence, for annealing temperatures over 365 °C, i.e. for the total crystallization of the PbF_2 phase, it proves that all the Er^{3+} ions are segregated into the crystallites.

Thus, the study of the unit cell parameter of the nanocrystallites demonstrates that the crystallites composition is $Pb_{0.82}Er_{0.18}F_{2.18}$ whatever the PbF_2 crystallization rate. It corresponds to the total segregation of Er^{3+} ions inside the crystallites when the PbF_2 crystallization is complete, i.e. for annealing temperatures over 365 °C.

3.3. Size and morphology of the nanocrystallites

The XRD diagrams of the glass-ceramics also allowed calculating the average size L of the nanocrystallites using Scherrer formula. However, one can notice that the linewidth also integrate all the broadening causes such as defects and strains induced by the surrounding glassy phase.

Four Bragg peaks labelled (111), (200), (220) and (311) were used to estimate the average size of the crystallites (Table 1). Higher the annealing temperature, bigger the crystallites. Annealing at high temperature favors the dissolution of the smaller crystallites at the benefit of the growth of the larger ones. This coarsening process is often called Ostwald ripening [16].

TEM images of three glass-ceramics resulting from heat treatments at 355, 365 or 395 °C were done. The micrographs of two of them, recorded in dark field, are represented in Fig. 5. One can observe numerous spherical crystallites, in black and white, and the amorphous phase, corresponding to the grey background. The crystallites size was evaluated through images analysis of the TEM micrographs. The average size of the sample annealed at 355 °C was evaluated to be 16.0 ± 0.5 nm, which corresponds to the average value found by XRD measurements (15.8 nm, Table 1). For the sample resulting from a heat treatment at 365 °C, the crystallites size is 21.0 ± 0.5 nm, which is also in good agreement with the size calculated from its XRD diagram (19.8 nm). Concerning the sample annealed at 395 °C, the average size determined by TEM is 32.0 ± 0.5 nm, whereas the value found by XRD was 26.5 nm. This difference can be due to a slight broadening of the diffraction peaks, inducing a small overestimation of the particle size determined by XRD. This additional broadening might indicate the presence of disorder inside the crystallites for an annealing at 395 °C.

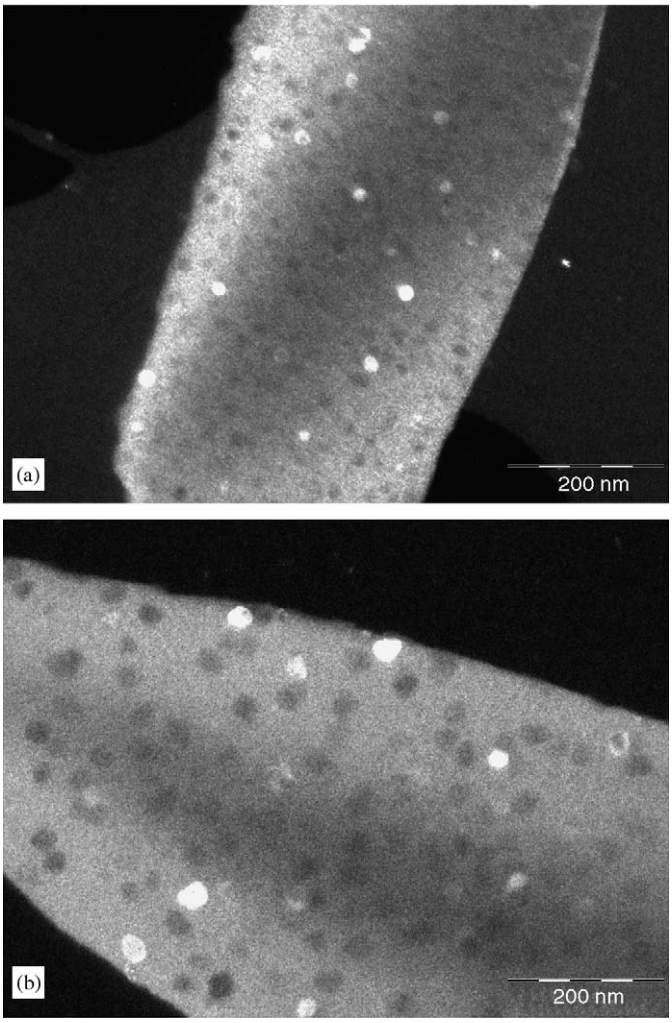

Fig. 5. Dark field TEM micrographs of glass-ceramics resulting from heat treatment at (a) 355 °C and (b) 395 °C.

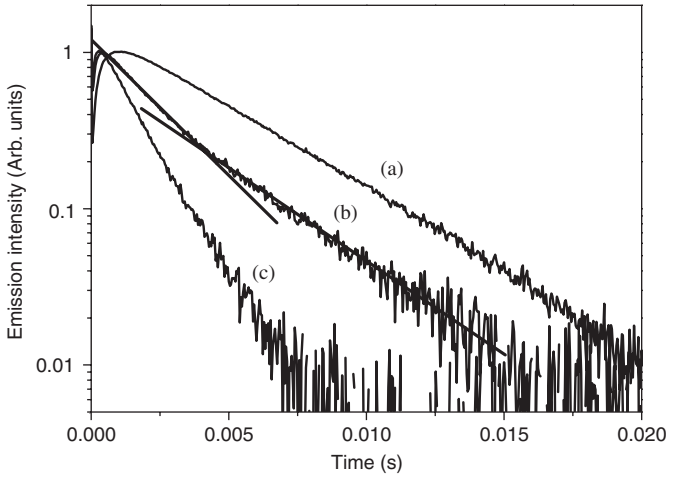

Fig. 6. Er^{3+} $^4I_{13/2}$ level decay curves of (a) the as-melted glass, (b) the glass-ceramic resulting from a 355 °C-heat treatment, (c) the glass-ceramic resulting from a 385 °C-heat treatment. Excitation (at 980 nm) is done in the $^4I_{11/2}$ level.

Table 2
Er^{3+} $^4I_{13/2}$ fluorescence lifetimes in the glass, glass-ceramics, and $Pb_{1-x}Er_xF_{2+x}$ bulk single crystals under study

Annealing temperatures	A_1' (%)	τ_1 (ms)	A_2' (%)	τ_2 (ms)
Glass	100	4.5±0.1	0	—
Glass-ceramic 350 °C	90	4.5±0.1	10	2.0±0.1
Glass-ceramic 355 °C	50	4.5±0.1	50	2.0±0.1
Glass-ceramic 360 °C	40	4.5±0.1	60	2.1±0.1
Glass-ceramic 365 °C	0	—	100	2.1±0.1
Glass-ceramic 370 °C	0	—	100	1.9±0.1
Glass-ceramic 380 °C	0	—	100	1.7±0.1
Glass-ceramic 385 °C	0	—	100	1.6±0.1
Glass-ceramic 395 °C	0	—	100	1.7±0.1
$Pb_{0.8}Er_{0.2}F_{2.2}$ single crystal			100	2.5±0.1
$Pb_{0.91}Er_{0.09}F_{2.09}$ single crystal			100	6.0±0.1
$Pb_{0.98}Er_{0.02}F_{2.02}$ single crystal			100	11.1±0.1

3.4. Optical characterization

3.4.1. Er^{3+} $^4I_{13/2}$ energy level lifetime measurements

The Er^{3+} $^4I_{13/2}$ energy level lifetime in the as-melted glass, in the different glass-ceramics and in the bulk single crystals was measured by exciting at 980 nm, i.e. in the $^4I_{11/2}$ energy level. The fluorescence decay curves of the glass and of the two glass-ceramics, resulting from heat treatments at 355 or 385 °C, are represented in Fig. 6, in logarithmic scale. One can observe a rise time due to the excitation via the decay of the $^4I_{11/2}$ energy level followed by the decay of the $^4I_{13/2}$ energy level itself. In the following part, we will exclusively discuss the long-time portion of the curves, relative to the decay of the $^4I_{13/2}$ energy level. The $^4I_{13/2}$ fluorescence lifetime's values for the different samples studied are gathered in Table 2.

For the glass, one can notice that, the decay curve $I_f(t)$ is purely linear in logarithmic scale. It means that the fluorescence decay curve can be fitted with one single exponential: $I_f(t) = A_1 \exp(-t/\tau_1)$, with τ_1, the $^4I_{13/2}$ energy level lifetime in the glassy oxyfluoride environment, being equal to 4.5 ms. The $^4I_{13/2}$ decay times of the $Pb_{1-x}Er_xF_{2+x}$ bulk single crystals are also single exponentials and can be fitted to the expression $I_f(t) = A_2 \exp(-t/\tau_2)$. The fluorescence lifetime τ_2, characteristic of Er^{3+} in PbF_2 crystalline environment, decreases when the doping rate x increases. For $x = 0.2$, which is the erbium content of the nanocrystallites in the glass ceramic (see Section 3.2.3), the $^4I_{13/2}$ lifetime is equal to 2.5 ms.

For the glass-ceramic resulting from a reheating at 365 °C or above, the decay curves, in logarithmic scale, are also linear, with decay times τ_2 lying between 2.1 and 1.7 ms. It can be noticed that the Er^{3+} lifetimes in the PbF_2 nanocrystallites of the glass-ceramic are similar, but slightly different, to the Er^{3+} lifetime in the bulk single crystal with the same doping rate ($\tau_2 = 2.5$ ms).

For the glass-ceramics resulting from a heat treatment between 350 and 360 °C, the decay curves in logarithmic scale show two slopes (Fig. 6). The fluorescence decay curve needs to be fitted by the expression: $I_f(t) = A_1 \exp(-t/\tau_1) + A_2 \exp(-t/\tau_2)$, with $\tau_1 = 4.5$ ms and $\tau_2 = 2.0$ or 2.1 ms. In this glass-ceramic, one part of the Er^{3+} ions with lifetime τ_1 lies in the glass, whereas the other part with lifetime τ_2 lies in the nanocrystallites.

In addition to the parameters τ_1 and τ_2 for all the glass-ceramics and single crystals, two other parameters A_1' and A_2', defined as

$$A_1' = \frac{A_1}{A_1 + A_2} \times 100 \quad \text{and} \quad A_2' = \frac{A_2}{A_1 + A_2} \times 100$$

are gathered in Table 2. The parameters A_1' and A_2' do not quantitatively represent the proportions of Er^{3+} in one or the other environment, because they do integrate the transition probabilities and the absorption cross-sections of Er^{3+} ions which depend on their environment. Nonetheless, the evolution of A_1' and A_2' according to the annealing temperatures qualitatively reflects the evolution of the Er^{3+} proportion in the two phases of the samples. This demonstrates the biphasic nature of the glass-ceramics annealed between 350 and 360 °C, the complete crystallization of PbF_2 in the glass-ceramics heated above 360 °C and the total segregation of erbium in the lead fluoride nanocrystals. This is an independent confirmation of the DTA and XRD results presented above.

3.4.2. Comparison between Er^{3+} lifetime in the glass and PbF_2 crystals

It has already been pointed out that the $^4I_{13/2}$ level lifetime of Er^{3+} in the $Pb_{1-x}Er_xF_{2+x}$ bulk single crystals decreases when the doping rate increases (Table 2). For instance, the $^4I_{13/2}$ level lifetime decreases from 11.1 to 2.5 ms when Er^{3+} concentration increases by the factor

of 10. This behaviour, which is rather common in rare-earth-doped materials [17], results from ion–ion interactions in concentrated samples. These interactions: cross-relaxation and energy migration towards luminescence traps, provide new de-excitation channels for the fluorescent ions and the fluorescence lifetime decreases.

The $^4I_{13/2}$ level lifetime of Er^{3+} in the glass ($\tau_1 = 4.5$ ms) and in $Pb_{1-x}Er_xF_{2+x}$ can now be compared. The crystal with $x = 0.02$, which presents approximately the same Er^{3+} concentration than the glass, exhibit a much longer lifetime of 11.1 ms. This difference can be accounted for by considering that the phonon energy cut-off in oxides (about 900 cm^{-1} for germanate glass [18]) is much higher than in the fluorides (333 cm^{-1} in PbF_2 [19]). Consequently, the non-radiative de-excitation channels that contribute to the decrease of the $^4I_{13/2}$-excited state population are very efficient in the glass and thus diminish the fluorescence lifetime. On the contrary, this mechanism is inefficient in fluoride environment and the Er^{3+} fluorescence lifetime is longer, close to the radiative one assuming negligible ion–ion interaction in such a diluted $Pb_{0.98}Er_{0.02}F_{2.02}$ crystal.

We should also account for symmetry considerations and differences between the glass and the crystal. In the glass, the point symmetry should be considered to be high but with lower symmetry contributions to the crystal field allowing degeneracy removal [20]. It induces high electric dipole transition probability P, decreasing the radiative lifetime which is proportional to $1/P$. In $Pb_{1-x}Er_xF_{2+x}$ single crystals, the presence of purely cubic sites [21] leads to higher radiative lifetime.

3.4.3. Comparison between the Er^{3+} lifetime in the glass-ceramics and in the $Pb_{0.8}Er_{0.2}F_{2.2}$ bulk single crystal

For an annealing of the glass at 365 °C, the Er^{3+}-doped PbF_2 phase has completely crystallized in the glass-ceramic and the $^4I_{13/2}$ fluorescence lifetime is 2.1 ± 0.1 ms. For comparison, the $^4I_{13/2}$ level lifetime, measured in $Pb_{0.8}Er_{0.2}F_{2..2}$ bulk single crystal having the same composition (see Section 3.2.3) is 2.5 ± 0.1 ms, which is close but slightly different from the value found for the nanocrystallites.

The difference can result from the effect of the matrix on the Er^{3+} ions contained in nanocrystallites. Several studies have proved that the oxide glassy matrix interacted with the rare-earth ions situated inside the nanosized crystallites and influenced their spectroscopic properties [22,23]. First, Er^{3+} ions, close to the surface of the nanocrystallites, are in distorted sites, compared to those in the bulk that lie in the cubic sites [24]. The distortions, lowering the symmetry, could increase the electric dipole transition probability P, thus decrease the radiative lifetime. Second, rare-earth ions close to the surface of the crystallites can be sensitive to the presence of oxide ions in their coordination polyhedron, inducing multi-phonons non-radiative contribution to the Er^{3+} de-excitation and lowering the fluorescence lifetime.

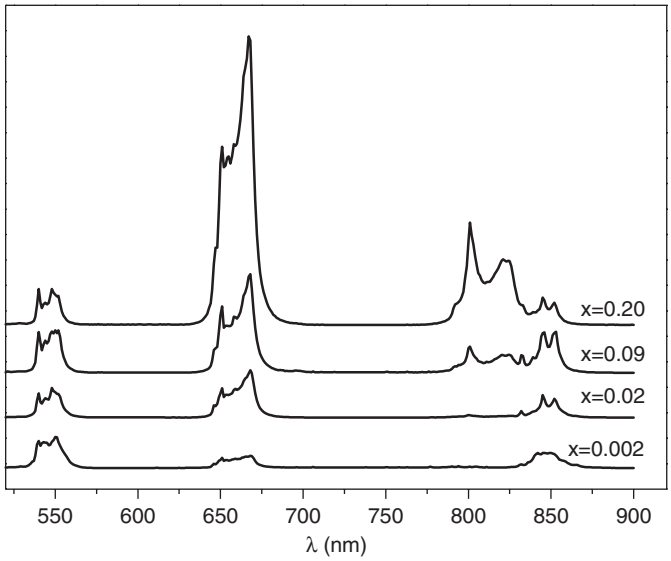

Fig. 7. Fluorescence spectra of $Pb_{1-x}Er_xF_{2+x}$ single crystals, according to the Er^{3+} doping rate x. $\lambda_{excitation} = 488$ nm, at room temperature.

3.4.4. Visible and NIR emission spectra

3.4.4.1. Case of the single crystals. The fluorescence spectra of the $Pb_{1-x}Er_xF_{2+x}$ bulk single crystals were recorded, under a CW 100-mW excitation at 488 nm, populating the $^4F_{7/2}$ Er^{3+} level. These spectra are shown in Fig. 7 and the Er^{3+} energy levels diagram is presented in Fig. 8.

The emission intensity of all the samples has been normalized on the green 550-nm emission band, resulting from the radiative de-excitation from the $^2H_{11/2}$ and $^4S_{3/2}$ levels (in thermal equilibrium and therefore both populated) to the $^4I_{15/2}$ ground state. Fig. 7 shows that the 850-nm emission intensity is quite similar for all the single crystals, meaning that this emission comes from the same energy level as the normalized 550-nm emission, i.e. the $^2H_{11/2}$ and $^4S_{3/2}$ energy levels. Hence, the 850-nm emission corresponds to the $(^2H_{11/2}, {}^4S_{3/2}) \rightarrow {}^4I_{13/2}$ transition. On the contrary, the intensity of the bands at 660 and 810 nm, corresponding respectively to the emission from the $^4F_{9/2}$ and the $^4I_{9/2}$ levels down to the ground state, varies according to the Er^{3+} doping rate x.

Higher the Er^{3+} doping rate x, stronger the emission bands at 660 and 810 nm, meaning that the population of the emitting energy levels $^4F_{9/2}$ and $^4I_{9/2}$ increases with the Er^{3+} content. Although the $^2H_{11/2}$ and $^4S_{3/2}$ level are populated through non-radiative de-excitations from the $^4F_{7/2}$ level (energy gap $\sim$1000 cm^{-1}), the $^4F_{9/2}$ and $^4I_{9/2}$ levels are populated either by radiative processes from the $^4F_{7/2}$ or $^4S_{3/2}$ levels or more likely by cross-relaxations between neighbouring Er^{3+} ions [25]. Some cross-relaxation processes involved in the population of these levels are represented in dashed lines in Fig. 8. For example, the $^4F_{9/2}$ level may be populated through the cross-relaxation scheme $(^4F_{7/2}–{}^4I_{11/2}) \rightarrow (^4F_{9/2}–{}^4F_{9/2})$. The cross-relaxation processes are enhanced when the Er^{3+} concentration

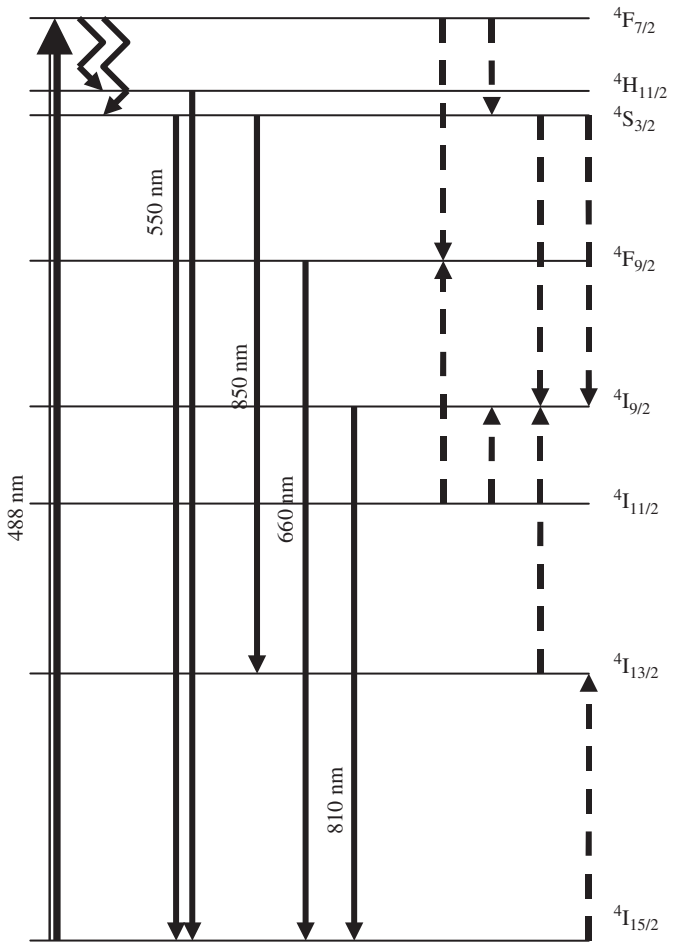

Fig. 8. Energy levels diagram of Er^{3+}, evidencing the emitting transitions (solid arrows), non-radiative relaxations (↯) and some possible cross-relaxation schemes processes (dashed arrows).

increases [25] because of the shortening of the Er^{3+}–Er^{3+} distances. Furthermore, it is known that, at high rare-earth content in Er^{3+}-doped MF_2 materials (M = Pb, Ca, Sr, Ba, Cd), Er^{3+} clusters are formed, leading to further shortening the Er^{3+}–Er^{3+} distances [21,26,27]. As a result, the $^4F_{9/2}$ and $^4I_{9/2}$ levels are more populated at higher Er^{3+} concentrations, increasing the emission bands intensity at 660 and at 810 nm at the expense of the 550-nm green emission.

3.4.4.2. Case of the glass-ceramics. The fluorescence spectra of two glass-ceramics samples annealed at 370 and 395 °C, as well as the spectrum of $Pb_{0.8}Er_{0.2}F_{2.2}$ bulk single crystal, are reported in Fig. 9. The recording was done under a CW 1-W excitation at 488 nm. As before, the emission spectra were normalized on the 550-nm emission band. The spectra of the nanocrystals and of the bulk single crystal are directly comparable because their erbium content is the approximately same ($x = 0.20$).

It appears that the relative intensities of the 660 and 810-nm emissions increase, with respect to the green 550-nm one, in the order: glass-ceramic 370 °C < glass-ceramic 395 °C < single crystal. Two contributions can explain this evolution:

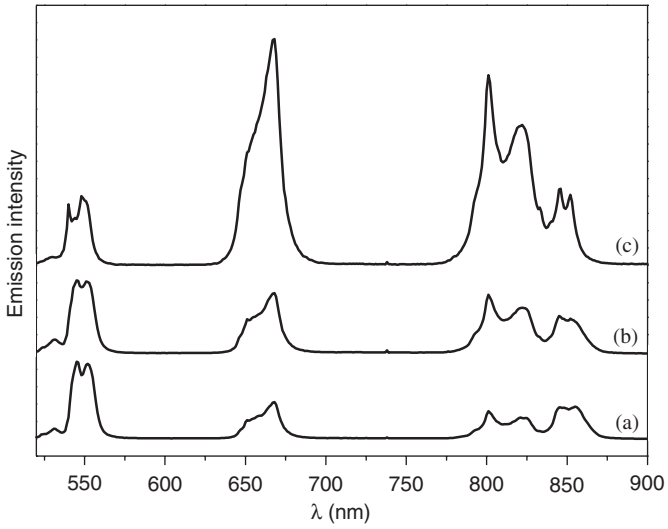

Fig. 9. Fluorescence spectra, under 488-nm excitation, of glass-ceramics resulting from annealing at 370 °C (a) and 395 °C (b) and $Pb_{0.8}Er_{0.2}F_{2.2}$ bulk single crystal (c). Recorded at room temperature.

- Non-radiative de-excitation processes occurring from the $^4F_{7/2}$ energy level, which populate the $^2H_{11/2}$ and $^4S_{3/2}$ energy levels, responsible for the green 550-nm emission. They are favoured for Er^{3+} ions lying near the surface of the nanoparticles of the glass-ceramic, with oxygen atoms in their coordination sphere providing high-energy phonons. Since the nanoparticles size increases with the annealing temperature (Table 1), the non-radiative processes increase in the order: single crystal < glass-ceramic 395 °C < glass-ceramic 370 °C.
- Cross-relaxations between neighbouring erbium ions processes, which populate $^4F_{9/2}$, $^4I_{9/2}$, … energy levels, leading to the increase of the 660- and 810-nm emission bands intensity with regard to the 550-nm one. When the materials are heated at high temperatures, the ion's mobility increases. As mentioned earlier, rare-earth ions usually associate into clusters and the Er^{3+}–Er^{3+} distance are reduced, leading to stronger emissions at 660 and 810 nm. Such clusters formation would be in good correlation with the possible broadening of the diffraction peaks observed on the XRD diagrams as discussed earlier in Section 3.3. The cross-relaxation processes, and the 660- and 810-nm emissions, are expected to increase in the order: glass-ceramic 370 °C < glass-ceramic 395 °C < single crystal that is grown from the liquid phase at 1000 °C.

Both explanations are in agreement with the decrease of the $^4I_{13/2}$ energy level lifetime observed for high annealing temperatures in the glass-ceramics (Table 2, Section 3.4.1). Indeed, $\tau_2 = 2.1 \pm 0.1$ ms for the glass-ceramic resulting from an annealing at 365 °C while $\tau_2 = 1.7 \pm 0.1$ ms for an

annealing at 395 °C. First, in the latter, cross-relaxation processes must be promoted, leading to the decrease of the $^4I_{13/2}$ energy level lifetime. Second, the formation of Er^{3+} clusters would induce concentration quenching and would also decrease the lifetime of the $^4I_{13/2}$ energy level. Moreover, energy migration and transfer to killing centres could occur.

4. Conclusion

The annealing of an Er^{3+}-doped GeO_2–PbO–PbF_2 glass induces the crystallization of a $Pb_{1-x}Er_xF_{2+x}$ phase, forming an oxyfluoride glass-ceramic. The study of the unit cell parameter of the nanocrystallites and of Er^{3+} $^4I_{13/2}$ energy level lifetime, as well as the comparison with Er^{3+}-doped β-PbF_2 bulk single crystals demonstrated that, for a heat treatment over 365 °C for 10 h, the whole PbF_2 has crystallized and all the Er^{3+} ions are segregated into the crystallites. During the devitrification, the crystallites composition is always constant, confirming the nucleation/growth process for the formation of the crystalline phase. It was evidenced that the oxide matrix does not induce modifications on the unit cell parameter of the nanocrystals in the glass-ceramics. For the highest annealing temperatures, Er^{3+} clusters are probably formed inside nanocrystals, favouring cross-relaxation processes and promoting red emission at the expense of the green one.

References

[1] P.A. Tick, N.F. Borrelli, L.K. Cornelius, M.A. Newhouse, J. Appl. Phys. 78 (11) (1995) 6367.
[2] B.N. Samson, P.A. Tick, N.F. Borrelli, Opt. Lett. 26 (3) (2001) 145–147.
[3] F. Lahoz, I.R. Rodriguez-Mendoza, I. Iparraguirre, J. Azkargorta, A. Mendioroz, R. Balda, J. Fernandez, V. Lavin, Opt. Mater. 27 (2005) 1762–1770.
[4] S. Hendy, Appl. Phys. Lett. 81 (7) (2002) 1171–1173.
[5] M. Mortier, G. Patriarche, J. Mater. Sci. 35 (2000) 4849–4856.
[6] M.P.A. Silva, V. Briois, M. Poulain, Y. Messaddeq, S.J.L. Ribeiro, J. Phys. Chem. Solids 64 (2003) 95–105.
[7] L.L. Kukkonen, I.M. Reaney, D. Furniss, A.B. Seddon, Phys. Chem. Glass. 42 (3) (2001) 265–273.
[8] V.K. Tikhomirov, D. Furniss, A.B. Seddon, I.M. Reaney, M. Beggiora, M. Ferrari, M. Montagna, R. Rolli, Appl. Phys. Lett. 81 (11) (2002) 1937–1939.
[9] M. Mortier, J. Non-Cryst. Solids 318 (2003) 56–62.
[10] R. Higginbottom, J.E. Shelby, Phys. Chem. Glass. 39 (5) (1998) 281–285.
[11] A. Dib, S. Aléonard, M.Th. Roux, J. Solid State Chem. 52 (1984) 292–301.
[12] JSPDS Card. no. 77-1866 C, $\lambda_{K\alpha 1}$(Co) = 1.789 Å.
[13] G. Dantelle, M. Mortier, D. Vivien, G. Patriarche, J. Mater. Res. 20 (2) (2005) 472.
[14] J.M. Leger, J. Haines, A. Atouf, O. Schulte, S. Hull, Phys. Rev. B 52 (18) (2005) 13247–13256.
[15] M. Mortier, G. Patriarche, Opt. Mater. (2005) in press, doi:10.1016/j.optmat.2005.07.008.
[16] W. Ostwald, Z. Phys. Chem. 34 (1900) 495.
[17] B. Henderson, G.F. Imbusch, Optical Spectroscopy of Inorganic Solids, Clarendon Press, Oxford, 1989.
[18] H. Sun, L. Zhang, M. Liao, G. Zhou, C. Yu, J. Zhang, L. Hu, Z. Jiang, J. Lumin. 117 (2006) 179–186.
[19] M.J. Castiglione, M. Wilson, P.A. Madden, J. Phys.: Cond. Matter 11 (1999) 9009.
[20] M. Mortier, Y.D. Huang, F. Auzel, J. Alloys Compd. 300–3001 (2000) 407–413.
[21] S. Mho, J.C. Wright, J. Chem. Phys. 79 (8) (1983) 3962–3975.
[22] X. Wang, S.H. Huang, R. Reeves, W. Wells, M.J. Dejneka, R.S. Meltzer, W.M. Yen, J. Lumin. 94–95 (2001) 229–233.
[23] M.A. Flores-Gonzales, G. Ledoux, S. Roux, K. Lebbou, P. Pierriat, O. Tillement, J. Solid State Chem. 178 (2005) 989–997.
[24] R.S. Meltzer, W.M. Yen, H. Zheng, S.P. Feofilov, M.J. Dejneka, B. Tissue, H.B. Yuan, J. Lumin. 94–95 (2001) 217–220.
[25] A. Patra, C.S. Friend, R. Kapoor, P.N. Prasad, Chem. Mater. 15 (2003) 3650–3655.
[26] M.D. Kurz, J.C. Wright, J. Lumin. 15 (1977) 169–186.
[27] S.A. Kazanskii, A.I. Ryskin, A.E. Nikiforov, A.Y. Zaharov, M.Y. Ougrumov, G.S. Shakurov, Phys. Rev. B 72 (2005) 014127-1–014127-11.